Noise-enhanced Stickiness in the Harper Map

J.R. Homan[a] and J.D. Meiss[b]

Department of Applied Mathematics, University of Colorado, Boulder, CO 80309-0526, USA

(Dated: 19 January 2026)

The Poincaré recurrence statistic (PRS) measures the probability that a trajectory initiated in a phase space region will first return to that region, as a function of time. For deterministic, area-preserving maps with a mixture of regular and chaotic orbits, the stickiness of invariant tori and islands is responsible for a power-law decay in the PRS. We show that noise perturbations allow trajectories to access the interior of islands, enhancing their trapping effect and causing many orbits to take longer to return to a neighborhood of their initial conditions. The noisy PRS can then exhibit an extended tail on an intermediate timescale, which is eventually followed by an asymptotic exponential decay. We study a typical example, the Harper map, and compare distributions of trapping and visit times to islands with recurrence times to show the importance of noise in creating tails in the PRS. A simple finite-state Markov model of the dynamics confirms how this slower decay can be caused by noise permitting entry to previously inaccessible regions.

Keywords: chaotic transport, area-preserving map, random perturbations, power-law decay

[a]Electronic mail: Corresponding author: Jonathan.Homan@colorado.edu

[b]Electronic mail: James.Meiss@colorado.edu

Chaos is a prominent feature of deterministic dynamical systems and is often thought of as akin to randomness, leading to unpredictability and diffusive motion. We study the effects of non-deterministic noise on transport in Hamiltonian systems, in particular for an area-preserving map. For the deterministic case, such transport is prohibited by invariant tori. However, in the presence of noise, previously invariant regions of phase space become accessible. We examine how this affects transport by computing the Poincaré recurrence statistic, which measures the fraction of trajectories that have yet to return to a neighborhood of their initial conditions. We study how the trapping within the regular islands surrounding stable periodic orbits depends on the intensity of the noise. Such island chains can inhibit transport when the noise intensity is small, but this effect goes away for sufficiently large noise intensity over long time scales. We show this results in a correlation between trapping time near an island and recurrence time to a well-separated region. A simplified Markov model elucidates this behavior, showing that a slower decay is introduced when noise is introduced.

I. INTRODUCTION

The phase space for many Hamiltonian systems is a combination of chaotic and regular regions, typically separated by invariant tori. These can be either absolute barriers, when they are co-dimension one, or merely impediments to transport when they are of lower dimension (e.g., the phenomena of Arnold diffusion[1,2]). When perturbed by noise, such invariant structures are typically destroyed; nevertheless, if the noise is weak enough, these barriers can still be important.

Even for a deterministic system, when an invariant torus is destroyed it is often replaced by a partial barrier—a *cantorus*—through which transport can be slow. This phenomena has been mainly studied for area-preserving maps and Poincaré sections of two-degree-of-freedom Hamiltonians.[3–5] Cantori also enclose the island chains surrounding periodic orbits,

leading to a power-law decay of survival probabilities,

$$P(t) \sim t^{-\gamma},$$

that is characteristic of Hamiltonian dynamics with mixed regular and chaotic regions.[6–10] In this paper we study how noise can alter such power laws.

There have been many studies of the effect of noise on chaotic dynamics. Early papers studied the momentum diffusion coefficient for Chirikov's standard map,[11–13]

$$\begin{aligned} x' &= x + y' + \delta x, \\ y' &= y - \tfrac{k}{2\pi}\sin(2\pi x) + \delta y, \end{aligned} \tag{1}$$

on the phase space $M = \mathbb{T} \times \mathbb{R}$. Here, the noise, represented by the perturbation $(\delta x, \delta y)$, is often chosen from a Gaussian distribution with zero mean and standard deviation σ. When $k > 2\pi$, (1) can have stable accelerator modes: elliptic orbits that have linearly growing momenta, y_t. In this case, the momentum diffusion coefficient D of the deterministic system diverges. Noise causes D to become finite, since particles can diffuse out of the accelerating islands. Karney et al[13] show that in the presence of noise $D \propto \sigma^{-2}$; similar results also apply in higher dimensions.[14]

More recently, the effects of both Gaussian and uniformly distributed noise on transport for (1) was studied by da Silva et al[15] setting $\delta x = 0$. They considered $K \approx 4$, where there is essentially only one elliptic region around the fixed point at $(0, 0)$, and studied the cumulative recurrence time statistic $P(t)$ (see (8) below) to a chaotic region outside the island. When the noise is non-zero but small ($\sigma \lesssim 10^{-3}$), its presence causes an enhanced trapping over intermediate times before an eventual exponential decay of P at longer times. These authors argue that the slower decay of the recurrence statistic is due to trajectories being able to diffuse into islands that were previously inaccessible, as measured by a decrease in the Lyapunov exponent of chaotic trajectories. We will see in §III that the Harper map exhibits similarly enhanced trapping and will relate this enhancement to noise-induced trapping of orbits in islands in §IV. In the presence of noise, trajectories can enter regular islands and may have long orbit segments within the region, increasing the time before recurrence.

A related phenomenon is the effect of noise on escape for open dynamical systems. Examples include billiards with a "hole" in a boundary,[16] naturally unbounded systems like the Hénon-Heiles model,[17,18] and noise-induced escape from potential wells.[19] For polynomial maps such as the Hénon quadratic map, noise can cause previously bounded orbits to diffuse to the boundary of an island and then escape to infinity.[20] This is similar to the effect of noise on chaotic scattering.[21,22] In particular, noise can allow orbits within an elliptic region to escape (scattering) with an exponentially decaying distribution.[23] For uniformly hyperbolic dynamics, the escape rate is proportional to the (conditionally) invariant measure of the hole.[24]

In this paper we study the effect of random perturbations on the Harper map on the torus $M = \mathbb{T}^2$, as recalled in §II. Like (1), the Harper map exhibits normal and anomalous diffusion due to accelerator modes.[25] It has also been studied as an example of a non-twist map,[26] and—since it can be thought of as a time periodic composition of two shear flows—as a model for mixing of a passive scalar in a fluid.[27] In §II we discuss two cases that we will study in detail. One has many regular regions, including rotational invariant circles that separate the phase space. The second, which we refer to as "nearly ergodic," is much more chaotic but still has four small, visible regular islands. For a noise perturbation we choose, as in (1), additive, normally distributed noise.[a]

We will use several notions of recurrence and transit times that are formalized in §III. In §III A-§III B we study the Poincaré recurrence distribution to a small region near the hyperbolic fixed point of the map, showing that the addition of noise can, surprisingly, lead to long-time tails on the recurrence distribution. In §IV we develop several techniques for detecting the importance of islands on these distributions. Finally in §V, we propose a simple finite-state Markov model, where one state represents an invariant region of the deterministic case, to elucidate the noise-induced tails.

[a] We show in Appendix A that uniformly distributed noise, and "post hoc" noise both give results that are essentially indistinguishable from the Gaussian case. Thus we primarily study Gaussian noise.

II. HARPER MAP MODEL

In this paper we will consider noisy perturbations to the well-known Harper map,[25,26,28–31] $H : \mathbb{T}^2 \to \mathbb{T}^2$, defined by

$$\begin{aligned} y' &= y + \tfrac{K}{2\pi}\sin(2\pi x), \\ x' &= x - \tfrac{L}{2\pi}\sin(2\pi y'). \end{aligned} \tag{2}$$

Two typical phase portraits for this deterministic map are shown in Fig. 1. For panel (a), where $(K, L) = (0.6, 4)$, the phase space is divided into two major components by two bands of rotational invariant circles (each surrounds a twistless invariant circle[26]). There are also many island chains; the largest surround the fixed points at $(0, 0)$ and $(\frac{1}{2}, \frac{1}{2})$. In Fig. 1(b), with $(K, L) = (1, 5)$, the dynamics appears to be more "nearly ergodic." There are now only four visible islands that surround a pair of elliptic period-two orbits: the highest and lowest islands (red in Fig. 1) comprise one chain, and the pair near $(\frac{1}{2}, \frac{1}{2})$ make up another. These arise from period doubling bifurcations of the fixed points. However, note that even though all the rotational invariant circles in this phase portrait have been destroyed, they have been replaced by cantori, some of which still have relatively low flux. Since the initial conditions are in the box Λ near the hyperbolic fixed point $(0.5, 0)$, the central region, $0.2 \lesssim y \lesssim 0.7$, has fewer points along the orbits shown than its complement. Though these trajectories do eventually cross the cantori separating the two regions, but this occurs only after many iterates.

Adding a noise perturbation to (2) results in the map $f_\sigma : \mathbb{T}^2 \to \mathbb{T}^2$,

$$\begin{aligned} y' &= y + \tfrac{K}{2\pi}\sin(2\pi x) + \delta y, \\ x' &= x - \tfrac{L}{2\pi}\sin(2\pi y') + \delta x, \end{aligned} \tag{3}$$

where $(\delta x, \delta y)$ are random perturbations. Note that the noise in (3) is added first to the y-component, and this value is then used in computing x. Many studies use this formulation.[13,14] As usual, we denote an orbit of a realization of f_σ by a sequence $\{(x_t, y_t),\ t = 0, 1, \ldots\}$ such that

$$(x_{t+1}, y_{t+1}) = f_\sigma(x_t, y_t). \tag{4}$$

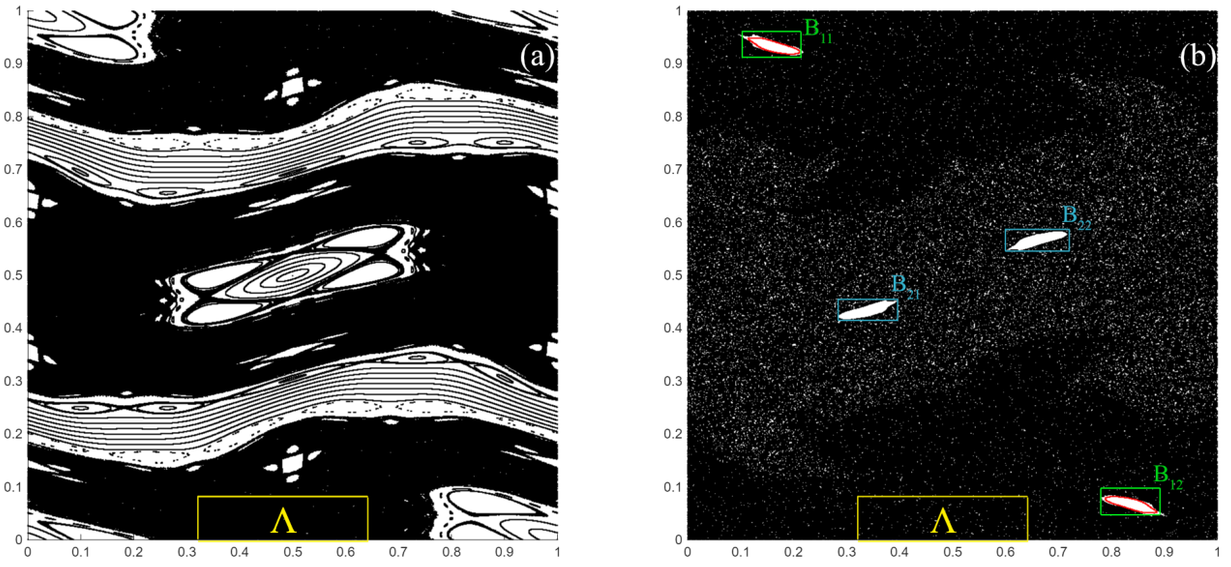

FIG. 1: Phase portraits for the Harper map (2) with (a) $(K, L) = (0.6, 4)$, and (b) $(K, L) = (1, 5)$. For (a), there are 100 initial conditions on the line $x_0 = y_0$ and each is iterated $t = 3(10)^4$ steps. For (b), the 200 initial conditions are on the line segment $(x_0, 0)$, with $0.4 \leq x_0 \leq 0.6$, iterated to $t = 3000$. A period-two island chain is identified in red. The boxes Λ, (13) (yellow), $\mathcal{B}_{11}$, $\mathcal{B}_{12}$, (16) (green), and $\mathcal{B}_{21}$, $\mathcal{B}_{22}$ (17) (blue) used in §III and §IV are also shown.

We assume that the random forcing in (3) has zero mean and standard deviation σ. We will primarily assume that the noise has a Gaussian distribution with zero mean:

$$\delta x, \delta y \sim \mathcal{N}(0, \sigma^2). \tag{5}$$

The effects of using several other noise distributions are discussed in Appendix A.

III. RECURRENCE TIME STATISTICS

To characterize transport from a given region $\Lambda \subset \mathbb{T}^2$ to another $\Omega \subset \mathbb{T}^2$ we define the *cumulative transition statistic*,[32–35]

$$C(t; \Lambda \nrightarrow \Omega) = \text{prob}\left(f_\sigma^j(x, y) \notin \Omega,\ \forall j \in [1, t] \,|\, (x, y) \in \Lambda\right), \tag{6}$$

i.e., the probability that a trajectory initialized in Λ has not yet entered Ω by time t. Note that C decreases monotonically and that in particular, $C(t) = 1$ for all t if there is an invariant set separating Λ and Ω. We numerically estimate (6) as

$$C(t; \Lambda \nrightarrow \Omega) \approx \frac{N(t)}{N(0)}. \tag{7}$$

Here, $N(0)$ is the number of randomly chosen initial conditions in Λ, and $N(t)$ is the number of those trajectories that have not yet entered Ω by time t.

For the case $\Omega = \Lambda$, C becomes the *Poincaré recurrence time statistic*[b] (PRS), the fraction of orbits that have **not** returned to Λ by time t:

$$P(t; \Lambda) = C(t; \Lambda \nrightarrow \Lambda). \tag{8}$$

To compute P, we take $N(t)$ in (7) as the number of trajectories started in Λ that have not reentered Λ by time t.

It is also convenient to define the first return or *recurrence time*, $t^R : \Lambda \to \mathbb{N}$:

$$t^R(x, y; \Lambda) = \min_{j \geq 1} \{j \mid f_\sigma^j(x, y) \in \Lambda\}. \tag{9}$$

By the Poincaré recurrence theorem, the set of points that never recur, where $t^R = \infty$, has zero measure. Moreover, Kac's theorem implies that for a measure preserving map, the mean recurrence time is

$$\langle t^R(x, y; \Lambda) \rangle = \frac{\mu(\Lambda_{acc})}{\mu(\Lambda)} \tag{10}$$

where μ is the invariant measure, and $\Lambda_{acc} \subset M$ is the region that is accessible to orbits that start in Λ.[36]

Using the indicator function for a set B, 1_B, we also define the *cumulative trapping time*, $t^T : \mathbb{T}^2 \times \mathbb{N} \to \mathbb{N}$:

$$t^T(x, y, k; B) = \sum_{j=0}^{k} 1_B(f_\sigma^j(x, y)). \tag{11}$$

[b] Also called the recurrence time distribution (RTD)[34] or statistic (RTS)[15].

Thus t^T is the total time that a trajectory starting at (x, y) spends in B up to time k. Finally, we define the *cumulative number of visits* to a region B for a single trajectory, $n^V : \mathbb{T}^2 \times \mathbb{N} \to \mathbb{N}$:

$$n^V(x, y, k; B) = \sum_{j=1}^{k} 1_B(f^j(x, y)) 1_{\mathbb{T}^2 \setminus B}(f^{j-1}(x, y)), \tag{12}$$

i.e., the number of times the trajectory segment $\{f^j(x, y) | \, j = 1, \ldots, k\}$ enters B from the outside. Of course $n^V \leq t^T$, since a trajectory might remain in B for more iterates after its initial entry to the region.

A. Computing the Poincaré Recurrence Statistic

For the parameters shown in Fig. 1, we will use the box

$$\Lambda = \{(x, y) \, | \, 0.32 \leq x \leq 0.64, \, 0 \leq y \leq 0.08\}, \tag{13}$$

to compute the cumulative Poincaré recurrence statistic (8). Note that Λ is a region near the hyperbolic fixed point at $(0.5, 0)$, and—for both cases—appears to contain only chaotic trajectories for the deterministic system. In the following sections, whenever we use the box (13) for the recurrence region, we will omit Λ in our notation: $P(t) = P(t; \Lambda)$ unless $P(t; \Lambda)$ is necessary for clarity. To approximate the PRS, we use (7), with $N(0) = 10^8$ randomly chosen initial conditions uniformly distributed in Λ unless otherwise stated.

As a first experiment, we consider the Harper map with parameters $(K, L) = (0.6, 4)$ as shown in Fig. 1(a), applying Gaussian noise with standard deviation σ (5). The PRS curves for this case are shown in Fig. 2(a), comparing the deterministic case (dashed black curve) to the noisy cases with eight variances, $10^{-8} \leq \sigma^2 \leq 10^{-1}$ (solid colors).

The average recurrence time (9) is for the deterministic case, $\langle t^R \rangle = 12.91$. Note that this is consistent with Kac's Theorem: the accessible region, Λ_{acc}, for the deterministic case is outside the region bounded by the rotational invariant circles near $y = 0.25$ and 0.75 and outside the islands. Using 10^5 initial conditions within Λ and a 100×100 grid, we estimate

$\mu(\Lambda_{acc})$ to be 0.3571 by taking the sum of the areas of grid boxes inhabited by the trajectories after $3(10)^4$ time steps. Then (10) implies that

$$\langle t^R \rangle = \frac{0.3571}{\mu(\Lambda)} = 13.9492,$$

close to the observed value of 12.91.

While the PRS curves in Fig. 2(a) vary considerably in shape as σ^2 varies, the mean recurrence time is nearly constant $\langle t^R \rangle = 39.12 \pm 0.24$. The fact that the average varies so little with σ is consistent with the figure: by $t \approx 200$, more than 90% of the orbits have returned to Λ for all cases. To apply Kac's theorem to this case, we note that when $\sigma \neq 0$, the entire phase space is accessible so $\mu(\Lambda_{acc}) = 1$ and (10) implies that

$$\langle t^R \rangle = \frac{1}{\mu(\Lambda)} = 39.065.$$

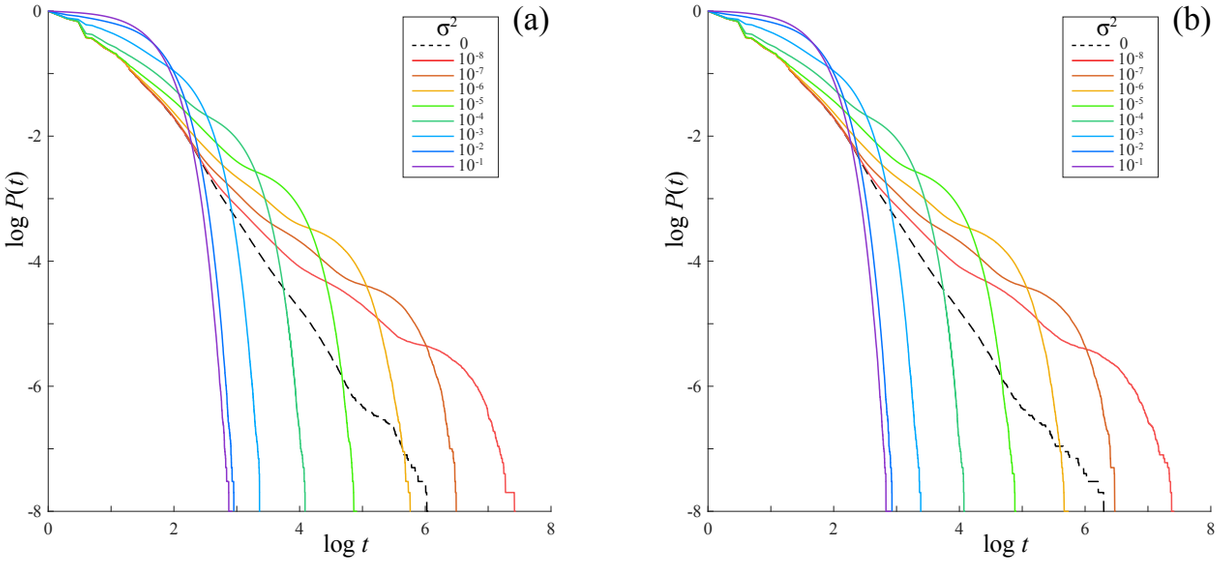

FIG. 2: Poincaré recurrence statistic (8) for the Harper map with $(K, L) = (0.6, 4)$: (a) Gaussian noise and (b) uniform noise (see Appendix A). Here we randomly choose $N(0) = 10^8$ initial conditions in Λ (13). Curves are colored according to the variance σ^2. Note that the deterministic cases (dashed) in the two panels differ slightly due to a different random seed for the choice of initial conditions in Λ.

The deterministic PRS in Fig. 2 appears to exhibit a power-law decay—a straight line on the log-log plot—with

$$P(t;\Lambda) \sim t^{-\gamma}, \quad \gamma \simeq 1.5587 \pm 0.0003, \quad 10 < t < 10^5. \tag{14}$$

Such power laws are characteristic of the stickiness of island chains and invariant circles in area-preserving maps[8,35,37] where a universal exponent $\gamma \simeq 1.56$ is predicted. For larger times, where $P \lesssim 10^{-6}$, the statistics of our computation become poor, since there are fewer than 100 nonrecurrent trajectories remaining. Thus, the deviation from the universal power law seen in the figure for $t \gtrsim 10^5$ is a sampling issue.

By contrast, when $\sigma > 0$ the PRS exhibits an eventual exponential decay

$$P(t;\Lambda) \sim e^{-\alpha t}, \; t \gg 1. \tag{15}$$

A similar decay has also been seen for the standard map[38]. Notice that when the variance is large, $\sigma^2 \geq 10^{-2}$, exponential decay begins immediately, but when $\sigma^2 < 10^{-2}$, the noisy PRS initially decays as a power law, similar to the deterministic case; this power law is eventually replaced by the exponential (15). A similar crossover has been reported for 1D maps.[39] We report least squares fits to these rates and the time intervals over which they apply in Table I; see Appendix B.

For the smallest variances, the initial decay of the noisy PRS follows the deterministic case for short times; for example, when $\sigma^2 = 10^{-8}$ they agree up to $t \approx 10^3$. However, as has also been observed by da Silva et al[15] for the standard map, the noisy PRS subsequently exhibits slower decay than the deterministic case over intermediate times. For example, when $\sigma^2 = 10^{-6}$ the noisy PRS follows the deterministic one for $0 < t < 100$ and then decays as $P(t) \sim t^{-0.879}$ up to $t \approx 4500$, much slower than the deterministic power law (14). This remarkable, slower decay also occurs for noise levels up to $\sigma^2 \sim 10^{-3}$, although, as shown in Table I in Appendix B, the power γ changes with the variance. For the smallest noise levels, the PRS has a tail that extends beyond that of the deterministic case, at least up to $t = 10^8$ where our computation stops. For each of the noisy cases the PRS eventually exhibits exponential decay, and when $\sigma^2 \geq 10^{-2}$ there is no observed time interval with power-law behavior.

B. Nearly Ergodic Case

Recurrence time distributions for the nearly ergodic case of Fig. 1(b), where $(K, L) = (1, 5)$, are shown in Fig. 3. Recall that for these parameters the deterministic map (2) has only four visible islands. These are completely inaccessible to orbits in their exterior; nevertheless, they should still exhibit the stickiness that gives rise to a power-law decay similar to (14).

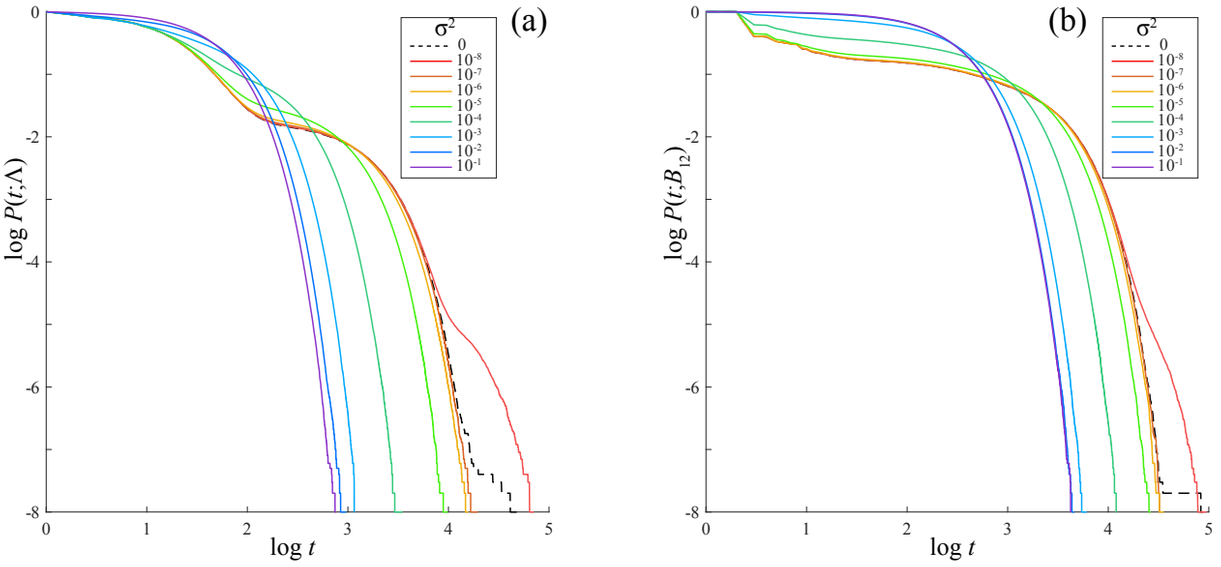

FIG. 3: Poincaré recurrence statistic $P(t)$ for the Harper map (3) with $(K, L) = (1, 5)$ and Gaussian noise (5) with variance σ^2. Panel (a): $P(t; \Lambda)$—trajectories are started in Λ (13). Panel (b): $P(t; B_{12})$—trajectories are started in B_{12} enclosing one of the period-two islands in Fig. 1(b).

The PRS $P(t; \Lambda)$ for the deterministic dynamics for this nearly ergodic case (black dashed curve in Fig. 3(a)) does not show (an obvious) power-law decay over our computation time: it appears to be a combination of two exponentials (15). Similar "hyper-exponential" distributions were used by Lozej[38] to fit recurrence time statistics for the deterministic standard map. Fits to these and the time intervals over which they apply are given in Table II in Appendix B. Though this PRS should—ultimately—exhibit power-law behavior, seeing this would require many more initial conditions and much longer iteration times.

As we saw in §III A, the noisy PRS eventually decays more rapidly than the deterministic one when the variance is large, here $\sigma^2 \gtrsim 10^{-5}$. As before, when the variance decreases, there is some indication of a short-time slowdown of the decay, but it is not as prominent as before. For smaller variances the noisy PRS follows the deterministic one for increasingly long times. For example, $P(t;\Lambda)$ for $\sigma^2 = 10^{-7}$ is almost identical to the deterministic case up to $t \approx 2(10)^4$, where $P(t;\Lambda) \approx 10^{-7}$. However, for the smallest noise level, $\sigma^2 = 10^{-8}$, $P(t;\Lambda)$ exhibits a slower decay than the deterministic case for the longest times shown, $10^4 < t < 10^5$; this gives a third exponential rate, see Appendix B.

Thus, larger noise initially slows the decay of $P(t;\Lambda)$ on an intermediate timescale but eventually results in a faster decay than the deterministic case. However, at the smallest noise level and on this time scale, there is a tail in the PRS, causing it to decay more slowly than the deterministic case, just as we saw in Fig. 2. This phenomenon—as we will discuss in the next section—is due to the islands.

To study the effect of the choice of initial conditions on the PRS, we now replace the starting region Λ with the box B_{12} seen in Fig. 1(b), a rectangular region enclosing an island in one of the period-two island chains (the explicit coordinates are given below in (16)). The resulting PRS, $P(t;B_{12})$ is shown in Fig. 3(b). For the deterministic case, each initial condition within the island enclosed by B_{12} will iterate to the second island in the chain and then recur after two steps. This causes the initial drop off in $P(t;B_{12})$ seen in Fig. 3(b). Similarly, trajectories in the chaotic region just outside the island will also tend to recur at $t = 2$ due to the trapping effect of any island-enclosing cantori. At the largest noise intensities, the PRS plots for both recurrence regions resemble each other, with only one decay rate, indicative of noise dominating the deterministic dynamics. However, even at the smallest noise intensities, there is only one exponential rate seen here, in contrast to Fig. 3(a). As we will see for a simple Markov model in §V, this can be attributed to a lower fraction of the orbits that enter the central chaotic region located near $y = 0.5$.

The initial drop-off at $t = 2$ persists for the noisy cases up to $\sigma^2 \leq 10^{-5}$, but for larger noise levels, the initial island recurrence is masked and the noisy PRS curves initially decay more slowly than the deterministic case—just as we saw for trajectories started in Λ. Similarly to

panel (a), as the noise amplitude decreases, the PRS increasingly follows the deterministic case, until for the smallest noise level $\sigma^2 = 10^{-8}$, there a long-time tail near $t = 10^5$. Again, we will attribute this tail in to the noise-induced stickiness of the islands in §IV.

IV. NOISE-ENHANCED STICKINESS

We think of the long tails on $P(t;\Lambda)$ seen in Figs. 2-3 for small, nonzero variances as *enhanced stickiness*. One hypothesis that might explain the tails is that in the presence of small noise, trajectories are able to access the interior of islands that are inaccessible in the deterministic case. This is supported in the work of Ohshika et al[24] for the standard map, who argued that the effective Lyapunov exponent of a noisy, chaotic trajectory can be reduced from that of the deterministic case when islands can be breached. Similar results have been seen for the Josephson map with uniform noise.[40] This map has accelerator modes, and it was shown that the anomalous diffusion exponent can increase in the presence of noise due to orbits diffusing into these accelerator modes.

To understand this phenomena in more detail, we will study recurrence (9), trapping (11), and visit (12) time for the nearly ergodic case of §III B.

A. Trapping near an Island Chain

Our first goal is to compute the trapping time for the period-two island shown in red in Fig. 1(b). For computational simplicity we enclose the islands in a pair of boxes,

$$\begin{aligned} \mathcal{B}_{11} &= \{(x,y)\,|\,0.1013 \le x \le 0.2206,\ 0.9128 \le y \le 0.96\}, \\ \mathcal{B}_{12} &= \{(x,y)\,|\,0.78 \le x \le 0.89, 0.047 \le y \le 0.085\}, \end{aligned} \tag{16}$$

as sketched in Fig. 1. We let $\mathcal{B}_1 = \mathcal{B}_{11} \cup \mathcal{B}_{12}$ denote the region associated with this period-two chain.

As a first visualization of the island trapping, Fig. 4 shows a 2D histogram of trajectories that start in Λ, comparing the recurrence time $t^R(x,y;\Lambda)$ (9) with the cumulative trapping time in the islands $t^T(x,y,k;\mathcal{B}_1)$ (11), setting $k = t^R$. To do this, the data for 10^8 trajectories

is partitioned into 200×200 bins, where the bins are evenly spaced for $(\log(t^R+1), \log(t^T+1)) \in [0,5] \times [0,5]$. The resulting 2D histograms are shown for four noise levels in the figure. The colors represent n, the number of trajectories in each bin.

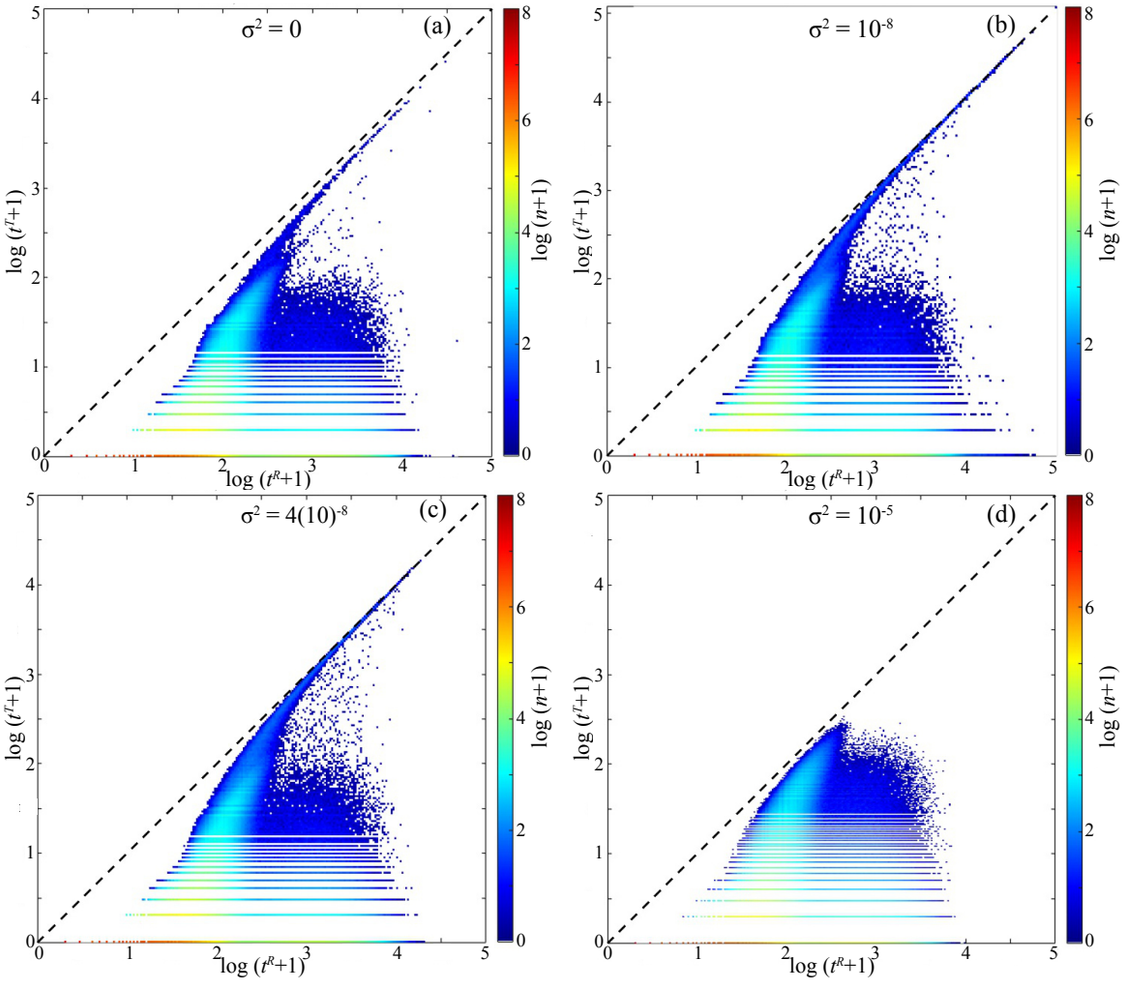

FIG. 4: Histograms of trapping time, t^T in $\mathcal{B}_1$ (16), versus recurrence time, t^R to Λ (13), for (3) with $(K, L) = (1, 5)$. The four panels correspond to variances (a) $\sigma^2 = 0$ (deterministic case), (b) 10^{-8}, (c) $4(10)^{-8}$, and (d) 10^{-5} with Gaussian noise (5). The dashed black line is $t^T = t^R$.

The axes (including the color bar) are all plotted logarithmically, which is the cause of the striations along the vertical axis for small t^T: the trapping time must be an integer. Since each variable in the histogram can be zero, we increment by one so that the logarithm is

non-negative. For example, when the population in a bin is zero, we have that $\log(n+1) = 0$, and these bins are colored white. For all noise levels, the maximum number of orbits in any particular bin is $\mathcal{O}(10^7)$; these are red in the figure. Most of the orbits have recurrence times in the range $1 \leq t^R \leq 200$, which is consistent with Fig. 3, since $P(200) \lesssim 0.015$. The diagonal line (dashed) in each of the plots signifies the maximum trapping time, since $t^T \leq t^R$.

For Fig. 4(b)-(c), where $\sigma^2 \leq 4(10)^{-8}$, there is a tail in the histograms for the orbits with the longest recurrence times,

$$t^T \sim t^R, \quad t^R \in [10^3, 10^5].$$

Trajectories in the tail tend to spend much of their time within the region $\mathcal{B}_1$. Though this effect is seen for the deterministic case in panel (a),

$$t^T \sim 0.75 t^R, \quad t \in [10^3, 10^4];$$

it is weaker and smaller. The stronger tail for small, nonzero σ shows the importance of noise in trapping trajectories in the interior of the island chain, which we will discuss further below.

B. Visits to an Island Chain

As a second illustration of the importance of the islands in trapping trajectories for the noisy map, we compute the cumulative number of visits, n^V (12), to the region $\mathcal{B}_1$ for $N(0) = 10^8$ trajectories started in Λ. A 2D histogram of visit versus trapping time, again with 200×200 log-bins, is shown in Fig. 5. As before, the black dashed line indicates the maximum: n^V cannot be greater than the trapping time. Note that trajectories with $n^V \sim t^T$ should not be considered trapped since they leave $\mathcal{B}_1$ as often as they visit.

For the deterministic case, Fig. 5(a), there is a tail in the histogram with

$$n^V \sim 0.178 t^T, \quad t^T \in [10^2, 10^4].$$

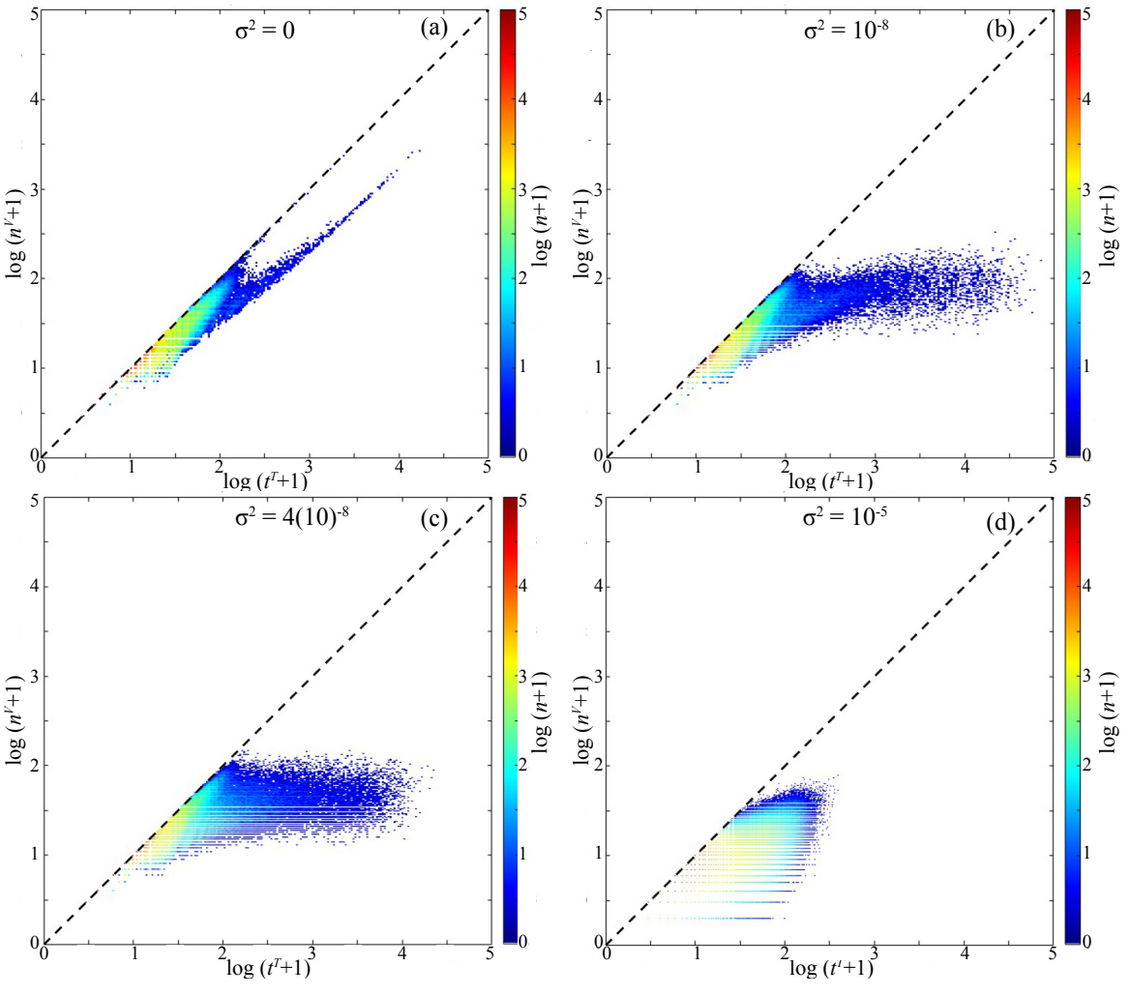

FIG. 5: Histogram of island chain visit instances, $n^V(x, y, t^R; \mathcal{B}_1)$ (12) as a function of $t^T(x, y, t^R; \mathcal{B}_1)$ (9) for the Harper map (3). As for Fig. 4, the four panels correspond to variances (a) $\sigma^2 = 0$ (deterministic case), (b) 10^{-8}, (c) $4(10)^{-8}$, and (d) 10^{-5}.

The implication is that although the longest trapped, deterministic orbits do *enter* $\mathcal{B}_1$, each such trajectory *remains* in $\mathcal{B}_1$, on average, for approximately five iterates. In other words, even though an island is "sticky," the probability of becoming entrained by the nested family of cantori with small fluxes surrounding the island is small. This is also consistent with the fact that we do not see a power law for the decay of $P(t)$ over the time range of Fig. 3.

Compared to the deterministic case, the noisy cases have a drastically different distribu-

tion for $t^T \gtrsim 10^2$. Trajectories that have a long trapping time now exhibit fewer visits to the island chain, resulting in a nearly flat tail. Though most trajectories do not visit $\mathcal{B}_1$ as we saw in Fig. 4, the ones that do are trapped for longer periods, as evidenced by their relatively small visit numbers compared to the overall trapping time. Once again, when the intensity of the noise is strong, in panel (d), the maximum trapping time is smaller and the distribution shifts towards the line $n^V = t^T$.

C. Trapping near a Second Island Chain

In Fig. 4, we saw that there is a population that does not spend much time trapped in the island chain $\mathcal{B}_1$ yet still exhibits long recurrence times. A possible cause is the influence of the second chain: recall that the nearly ergodic case of Fig. 1(b) has a pair of period-two islands. To understand the importance of this second chain we define two new boxes,

$$\begin{aligned} \mathcal{B}_{21} &= \{(x,y)\,|\,0.2821 \le x \le 0.3937, 0.4149 \le y \le 0.4539\}, \\ \mathcal{B}_{22} &= \{(x,y)\,|\,0.6 \le x \le 0.72, 0.545 \le y \le 0.585\}, \end{aligned} \tag{17}$$

that enclose the second pair of islands; these are the blue boxes in Fig. 1(b). Figure 6 shows trapping time versus recurrence time histograms for $\mathcal{B}_2 = \mathcal{B}_{21} \cup \mathcal{B}_{22}$. Once again, when noise is present, a population of trajectories spends increased time near the island chain, resulting in increased recurrence times. These histograms indicate that $\mathcal{B}_2$ is responsible for some of the "dust" of points below the main tail seen in Fig. 4. However, the trapping within $\mathcal{B}_2$ is less pronounced than that within $\mathcal{B}_1$: there is less correlation between t^R and t^T. We hypothesize that this occurs because, in order for a trajectory to move from Λ to $\mathcal{B}_2$, it must first cross the cantori that have replaced the rotational invariant circles of Fig. 1(a). By contrast, the region $\mathcal{B}_1$ is on the "same side" of the cantori as Λ and so is more easily visited by trajectories initialized in Λ. For the largest variance, shown in Fig. 6(d), the distribution is more t^T-independent, even more pronounced than that seen in Fig. 4(d) for $\mathcal{B}_1$.

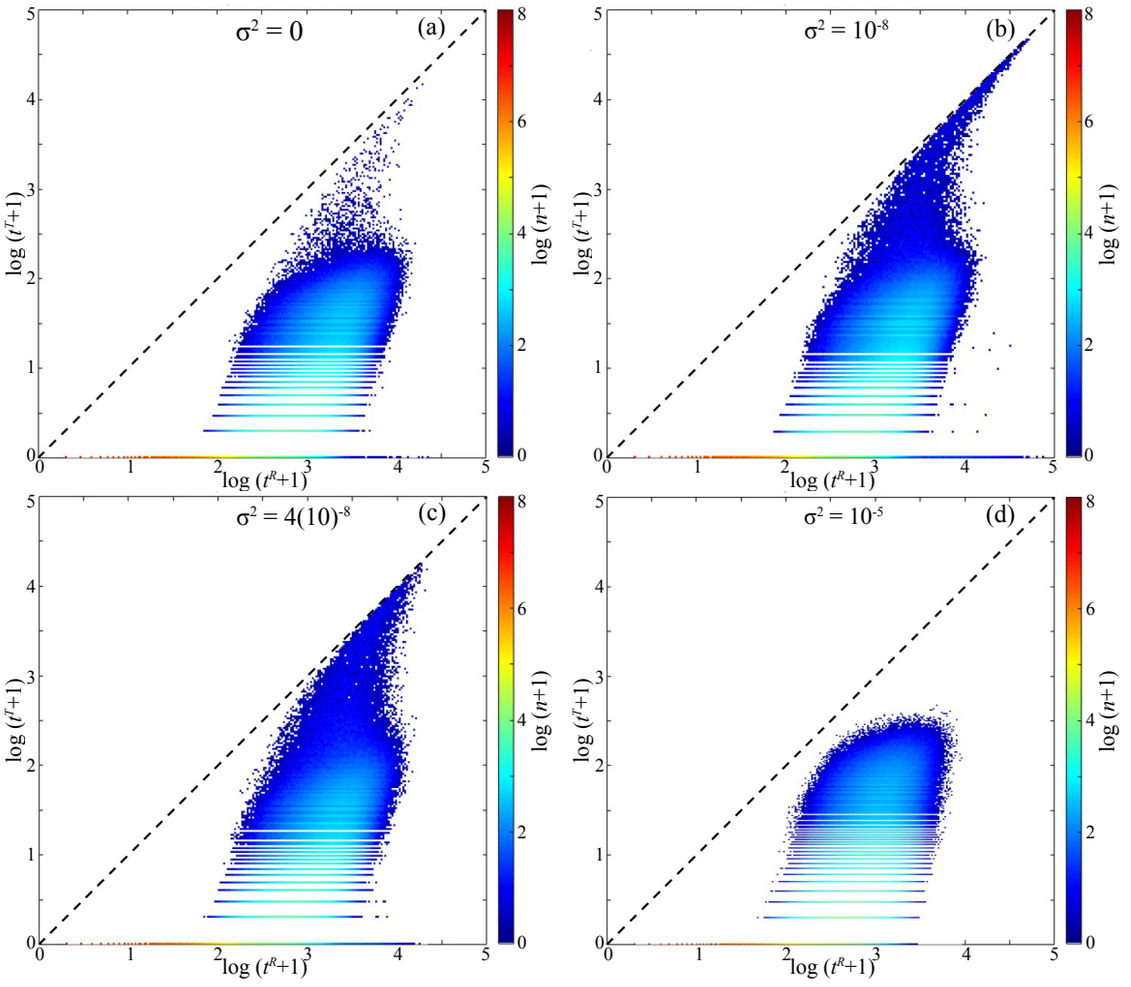

FIG. 6: Histogram of trapping time in the region $\mathcal{B}_2$ (17) versus recurrence time to Λ (13) for the noisy Harper map with $(K, L) = (1, 5)$. Noise levels are (a) $\sigma^2 = 0$, (b) 10^{-8}, (c) $4(10)^{-8}$, and (d) 10^{-5}. The dashed line indicates the maximum t^T for a given t^R.

D. Phase Space Structures

To visualize the phase space structure of orbits recurrent to Λ, Fig. 7 shows trajectories that *survive* up to $k = 100$, i.e., those with $t^R > 100$. Here we chose 10^5 initial conditions distributed uniformly in Λ for the nearly ergodic Harper map with $\sigma^2 = 0$ in panel (a), and $\sigma^2 = 10^{-5}$ in panel (b). As seen in the PRS (Fig. 3), there are more trajectories (4053)

that have not recurred at $t = k$ for $\sigma^2 = 10^{-5}$ than for the deterministic case (2775). Each point (x_t, y_t) in the first 100 iterates of a surviving orbit is colored by the current time t as shown in the color bar. Note that the phase points for the largest times (red) of most of these surviving orbits are either near $\mathcal{B}_1$ or within the region between the remnants of the rotational invariant circles. Thus, even though the cantori were not clearly visible in Fig. 1(b), we see that they have a strong influence on the surviving trajectories.

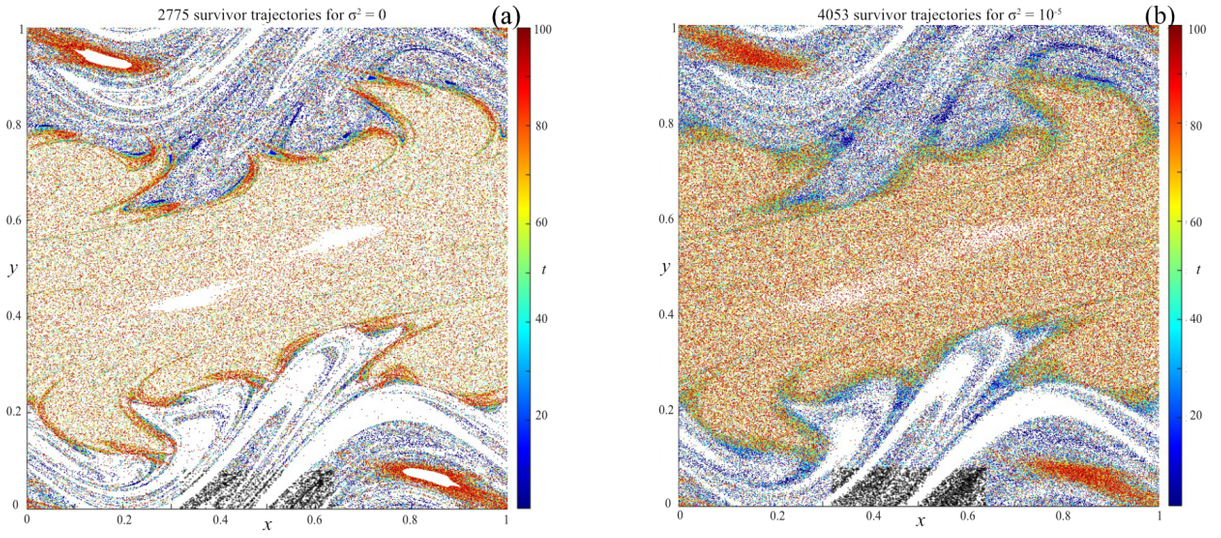

FIG. 7: Short-time survivors for $(K, L) = (1, 5)$. The first 100 iterates for trajectories with $t^R > k = 100$ for 10^5 initial conditions uniformly distributed in Λ. (a) The 2775 survivors for the deterministic case, and (b) the 4053 survivors for Gaussian noise with $\sigma^2 = 10^{-5}$. Each iterate is colored by the current time along the orbit; the initial conditions for these trajectories are the black points.

Figure 8 shows phase portraits for orbits with the longest recurrence times, $t^R > k = 3(10)^4$. Here we plot the *last* 100 iterates of such trajectories selected from 10^8 initial conditions in Λ. For the deterministic case in panel (a), only four trajectories survive: each is trapped at the edge of one of the period-two islands. For $\sigma^2 = 10^{-8}$ there are 115 surviving trajectories as shown in panel (b); these spend most of their last 100 iterates trapped *inside* one of the island chains.

These plots show how the stickiness of the islands correlates with the longest surviving

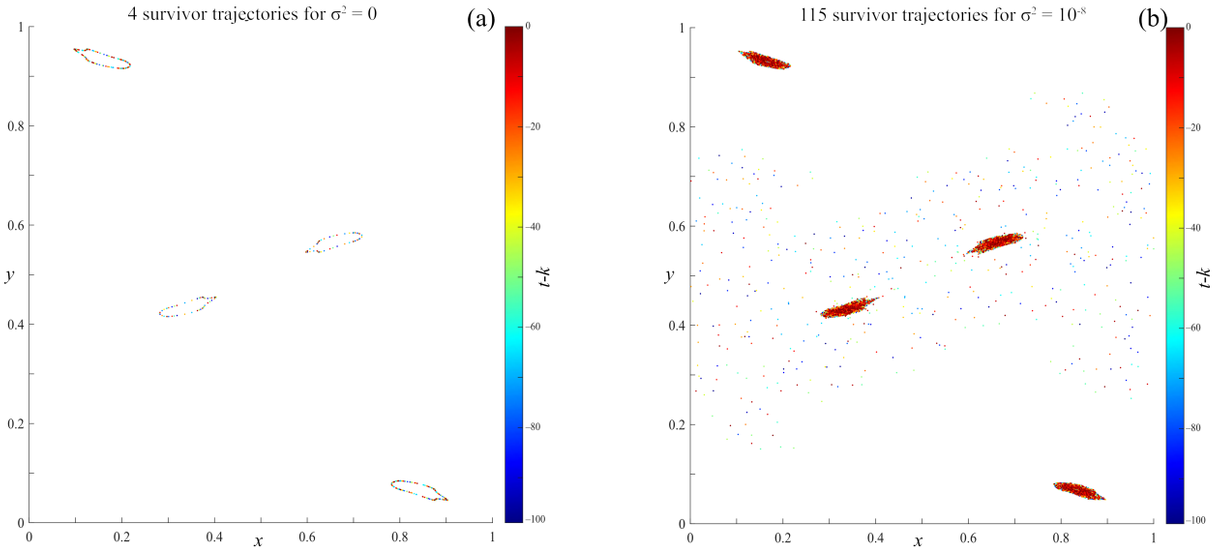

FIG. 8: Survivors of $N(0) = 10^8$ initial conditions in Λ with $t^R > k = 3(10)^4$, for $(K, L) = (1, 5)$. Shown are the final 100 iterates before $t = k$. (a) The four survivors for the deterministic case, and (b) the 115 survivors for Gaussian noise with $\sigma^2 = 10^{-8}$. Each point is colored by $t - k$, corresponding to the number of steps before k.

trajectories for small, but nonzero, noise. Even though a noisy trajectory can just as easily diffuse out of an island as it can diffuse in, we see that when the noise level is small, the longest recurrence times are correlated with trapping. The importance of islands is related to their size and the noise intensity. For a purely random process with noise (5), each component will undergo a random walk leading to a variance at time t of

$$\langle(\delta x(t))^2\rangle = \langle(\delta y(t))^2\rangle = \sigma^2 t,$$

since $\langle\delta x\rangle = \langle\delta y\rangle = 0$. Such a purely diffusive motion would lead to trajectories escaping islands of size ρ in a time of order

$$t_{escape} \sim \frac{\rho^2}{\sigma^2} \tag{18}$$

In the nearly ergodic case, the island chains have scale size $\rho \approx 0.03$. For the variance $\sigma^2 = 10^{-8}$ of Fig. 8(b), diffusive escape would occur at a time $t_{escape} \sim 9(10)^4 = 3k$, implying that the islands are still able to strongly influence trapping. It is worth noting that some of

the surviving trajectories in Fig. 8(b) are in the central chaotic region, outside of the island chains. These show the influence of the lower flux cantori in preventing recurrence to Λ.

A similar analysis for $(K, L) = (0.6, 4)$ is more complicated because there are many elliptic regions, as we saw in Fig. 1(a). Figure 9 shows the surviving orbits with $t^R > k = 1000$, for four noise levels. Note that as σ increases the number of survivors grows from 54 for the deterministic case to 926 for $\sigma = 10^{-2}$. As we saw before, the regular regions exhibit stronger trapping for small, nonzero noise. For example, the period-two chain near $(x, y) = (0, 0.15)$ and $(0.5, 0.15)$ traps more iterates for $\sigma^2 = 10^{-7}$, panel (b), than does the deterministic case, panel (a). However, when $\sigma^2 = 10^{-6}$, panel (c), this chain is less distinct, and at $\sigma^2 = 10^{-4}$, panel (d), it is no longer visible. For this noise level most of the surviving orbits have diffused across the bands of rotational invariant circles of the deterministic dynamics and are within the chaotic region $0.3 < y < 0.7$.

The period-two island chains in Fig. 9 have size $\rho \approx 0.04$. Using the estimate (18), we expect $t_{escape} \sim 2(10)^4$ for $\sigma^2 = 10^{-7}$, a long time on the scale of k. Consequently, trapping in these islands is prominent in Fig. 9(b). However, when $\sigma^2 = 10^{-4}$ in panel (d), $t_{escape} \sim 20$, implying—as seen in the figure—that these islands are not important at trapping orbits with $t^R > 1000$.

V. FOUR-STATE MARKOV MODEL

A simple explanation of the noise-induced stickiness observed in §IV can be obtained using a simplified, four-state Markov model of the dynamics. We suppose the phase space is divided into regions $\mathcal{F}, \mathcal{L}, \mathcal{G}$, and $\mathcal{B}$ with areas F, L, G, and B, respectively. This is a simplified model of the nearly ergodic case of §III B. We imagine that $\mathcal{F}$ and $\mathcal{G}$ correspond to large chaotic regions that are separated by relatively low-flux cantori, and $\mathcal{L}$ is the recurrence region (denoted Λ in §III) located in $\mathcal{F}$—we take it to be an absorbing state. The region $\mathcal{B}$ represents an island chain (like $\mathcal{B}_1$ discussed in §IV) surrounded by $\mathcal{F}$: thus, there will be no direct transitions between $\mathcal{B}$ and $\mathcal{G}$. For this simple model, we ignore any other structures in the phase space (such as the island chain $\mathcal{B}_2$ surrounded by $\mathcal{G}$), considering them to be

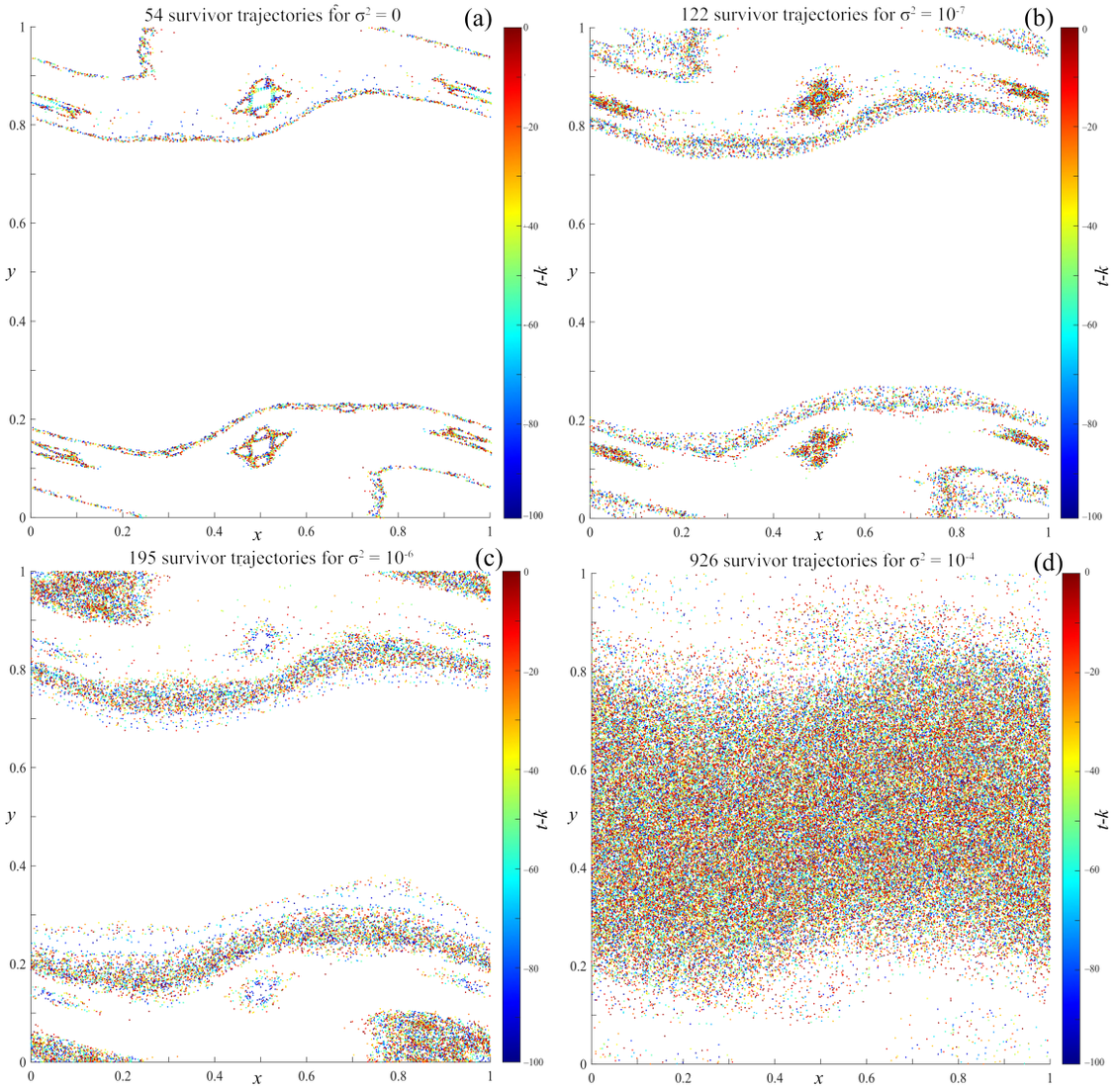

FIG. 9: Survivors from $N(0) = 10^5$ initial conditions in Λ with $t^R > k = 1000$, for $(K, L) = (0.6, 4)$. Shown are the final 100 iterates before $t = k$. Noise intensities are (a) $\sigma^2 = 0$, (b) 10^{-7}, (c) 10^{-6}, and (d) 10^{-4}, with each point colored by $t - k$ as indicated in the colorbar.

part of the chaotic regions they are located in. Our Markov model is structured to apply to a typical area-preserving map with regular regions, and so we expect the noise-enhanced tails of the PRS to exist for any such map.

For this interpretation, we assume that the total area is one, so $F + L + G + B = 1$, and

$F \approx G$ while B and L are small, so that

$$0 \leq B, L \ll F \leq G.$$

We let ΔW denote the deterministic flux between $\mathcal{F}$ and $\mathcal{G}$, and represent the noise by a flux ΔV, which will affect the flux between $\mathcal{F}$ and $\mathcal{G}$, as well as between $\mathcal{F}$ and $\mathcal{B}$. Since the fluxes represent the portion of the region that escapes per step, we assume that

$$0 \leq \Delta V \leq B < F, \quad 0 \leq \Delta W + \Delta V \leq \min(F, G)\ .$$

A Markov model for this simplified system is

$$\begin{pmatrix} \rho_L \\ \rho_F \\ \rho_G \\ \rho_B \end{pmatrix}' = \begin{pmatrix} 1 & \frac{L}{F+L} & 0 & 0 \\ 0 & 1 - \frac{L}{F+L} - \frac{\Delta W+\Delta V}{F} - \frac{\Delta V}{F} & \frac{\Delta W+\Delta V}{G} & \frac{\Delta V}{B} \\ 0 & \frac{\Delta W+\Delta V}{F} & 1 - \frac{\Delta W+\Delta V}{G} & 0 \\ 0 & \frac{\Delta V}{F} & 0 & 1 - \frac{\Delta V}{B} \end{pmatrix} \begin{pmatrix} \rho_L \\ \rho_F \\ \rho_G \\ \rho_B \end{pmatrix}. \tag{19}$$

Here the ρ's represent the density in each of the regions. As $\mathcal{L}$ is located within the chaotic region $\mathcal{F}$, we make the simplifying assumption that the regions mix quickly and uniformly; thus, the transition rate from $\mathcal{L}$ to $\mathcal{F}$ is proportional to L. This model also assumes that recurrence to $\mathcal{L}$ is only possible by a transition from $\mathcal{F}$, so that there is no immediate recurrence for trajectories in $\mathcal{G}$. In addition, we assume that the fluxes ΔW and ΔV are small enough so that the one-step probability of staying in $\mathcal{F}$ is positive, i.e., $\Delta W + 2\Delta V < \frac{F^2}{F+L}$.

For the first step of the Markov model, trajectories are allowed to escape from $\mathcal{L}$ through uniform mixing between $\mathcal{L}$ and $\mathcal{F}$. Thus we take the density at time 1 to be $\rho_1 = (\frac{L}{F+L}, \frac{F}{F+L}, 0, 0)^T$. Subsequently, we apply the transition matrix at each time step to obtain the PRS

$$P(t; \mathcal{L}) = \rho_F + \rho_G + \rho_B,$$

the sum of the densities in all states excluding the absorbing state $\mathcal{L}$.

The evolution of this PRS will be governed by the four eigenvalues of the transition matrix (19). It is trivial to confirm that

$$\lambda_L = 1, \quad \rho = (1, 0, 0, 0)^T,$$

is an eigenvalue-eigenvector pair, which corresponds to the absorbing set $\mathcal{L}$. An example of the dependence of the eigenvalues on the noise flux ΔV is shown in Fig. 10(a). Here, based on Fig. 7, we approximate the deterministic flux ΔW between regions $\mathcal{F}$ and $\mathcal{G}$ as 0.00028. We estimate $F + L \approx 0.5077$ by dividing up the phase space into 100×100 cells and computing the area of the cells occupied for 10^5 randomly selected initial conditions in $\mathcal{L}$ after 25 iterates, which avoids transitions into $\mathcal{G}$. The resulting relationship between ΔV and the eigenvalues of the transition matrix are plotted in Fig. 10(a).

For the deterministic case, $\Delta V = 0$ so the island region $\mathcal{B}$ is not accessible to trajectories initialized in Λ. In this case $\mathcal{B}$ is invariant and (19) has a second eigenvalue $\lambda_B = 1$, with the eigenvector $\rho = (0,\, 0,\, 0,\, 1)^T$. The remaining two eigenvalues are less than one and will govern the decay of the PRS, since we take the density in the state $\mathcal{B}$ to be initially zero. We denote these eigenvalues by $\lambda_- < \lambda_+ < 1$. This agrees with the computed PRS for the model in Fig. 10(b) when $\Delta V = 0$: the PRS is a hyper-exponential distribution with the rates $\lambda_- = 0.949$ and $\lambda_+ = 0.999$, for the parameters of the figure. Recall that we observed a similar, two-rate hyper-exponential distribution in Fig. 3(a) when the noise amplitude is zero. Indeed, using the fitted values in Table II for the deterministic Harper map, $\sigma^2 = 0$, gives $\lambda_- = e^{-\alpha_1} = 0.954$ and $\lambda_+ = e^{-\alpha_2} = 0.9991$, not far from the Markov model values.

The region $\mathcal{B}$, which represents the deterministic island, becomes accessible when $\Delta V > 0$. As seen in Fig. 10(a), as ΔV increases, λ_B monotonically decreases from 1. By continuity, there will always exist a range of ΔV values such that $\lambda_+ < \lambda_B < 1$. In other words, for small noise amplitudes, λ_B becomes the new slowest decaying eigenvector. The implication is that the PRS has a more slowly decaying tail when the noise is non-zero but small, due to the accessibility of an island. We observe this effect in Fig. 10, where the extended tail exists for $\Delta V < 5.8(10)^{-6}$. For larger noise amplitudes the ordering reverses, so that $\lambda_B < \lambda_+ < 1$ and the island-induced tail in the PRS goes away.

These features correspond to those we observed in Fig. 3: small noise can result in long time tails, but for larger noise these are absent. Our simple four-state model is not able to exactly replicate the decay rates seen in Fig. 3, since the model lacks some features, such as an island chain located within $\mathcal{G}$. This causes faster recurrence in our model; for example,

the model PRS is smaller for $t \approx 100$ than the actual PRS in Fig. 3(a).

To explain the behavior of the PRS in Fig. 3(b), we note that the central region corresponding to $\mathcal{G}$ is essentially inaccessible for trajectories when the recurrence zone $\mathcal{L}$ exhibits trapping effects (such as the island $\mathcal{B}_{12}$ (16)). Thus, the phase space for this case would have only two states (as the island region $\mathcal{B}$ is the recurrence region $\mathcal{L}$), resulting in a 2×2 transition matrix with only one eigenvalue less than one determining the decay rate of the PRS.

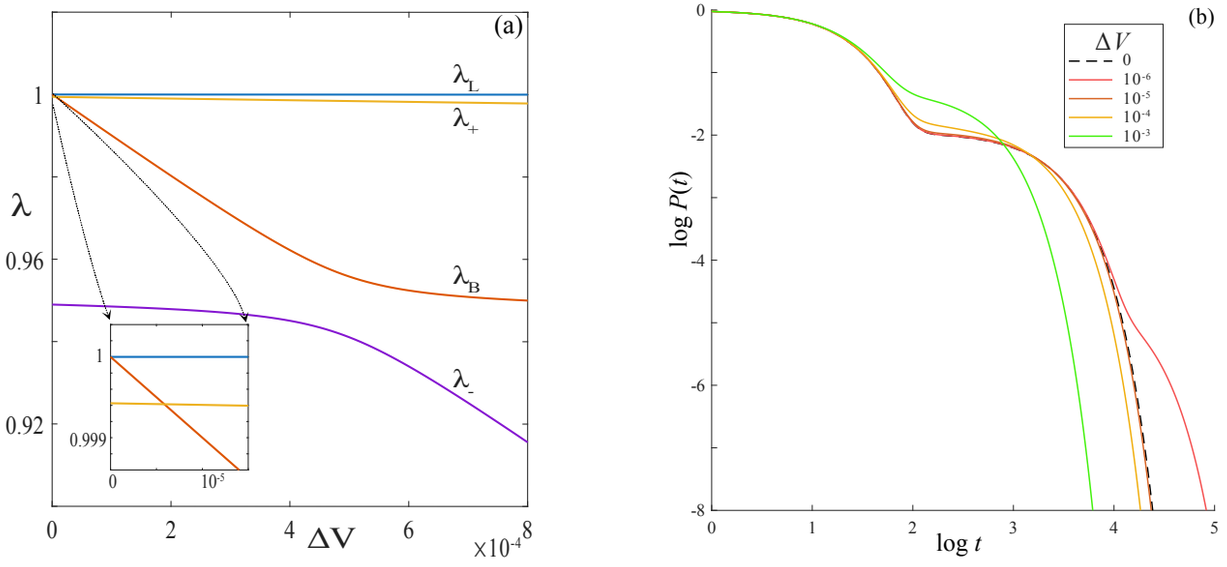

FIG. 10: Markov model for regions with areas $L = 0.0256$, $F = 0.4821$, $G = 0.4832$, $B = 0.01$, and flux $\Delta W = 2.8(10)^{-4}$. (a) Eigenvalues of the Markov model (19) as a function of the flux ΔV. (b) PRS for the Markov model for selected values of ΔV.

VI. CONCLUSIONS

We studied the structure of the Poincaré recurrence statistic (PRS) for two representative parameter sets of the Harper map (2) and how these depend upon added noise from three distinct distributions. For $(K, L) = (0.6, 4)$, where the deterministic map has a mixture of chaotic and regular regions, the noisy PRS shows a short-time power-law decay with a slower

rate than that characteristic of the deterministic case. On long time scales, the noisy PRS transitions to an exponential decay. For $(K, L) = (1, 5)$ the deterministic dynamics has only four small island chains, and we find that these are responsible for long-term trapping in the noisy case: trajectories with long recurrence times tend to spend most of their iterates near the islands, as seen in Figs. 4-6. When noise is added, trajectories can diffuse into the previous inaccessible islands, and this increases the recurrence times.

As noted by da Silva, Manchein, and Beims[15], the Chirikov standard map exhibits a similar behavior. They show that the Lyapunov exponent of chaotic trajectories can decrease with added noise, and this correlates with the extended tails in the PRS. We have seen that the island visit time and trapping time distributions in §IV give a more explicit demonstration of the stickiness of even small islands on the PRS. Indeed—even though a noisy trajectory can just as easily diffuse out of an island as it can diffuse in—when the noise level is small, the probability of leaving is also small. This leads to tails in the recurrence time distribution, as we saw in Fig. 3. However, when the noise intensity is larger, the exponential decrease in the PRS due to noise occurs on a shorter timescale. Orbits spend long periods of time trapped near the island chains when the noise intensity is small, and the distribution becomes more uniform when the noise intensity increases.

When the phase space has a more generic mixture of regular and chaotic orbits, it is harder separate the effects of individual structures; however, plots of the survivor trajectories, Figs. 7-9, still demonstrate the effects of noise on trapping. A simple estimate in §IV D, based on a random walk, confirmed that as long as the standard deviation from the deterministic trajectory is less than the size of the island, a noisy orbit will stay trapped by the island.

The simple Markov model of this phenomenon in §V showed that when an island becomes accessible due to noise, a new slowest decaying eigenvalue appears. This is consistent with the noise-induced slowing of the decay seen in the computations of §III. The eigenvalue decreases from one as the noise intensity grows, resulting in a new rate of decay for small noise intensities. We expect this result to apply to area-preserving maps in general.

Further refinement of the Markov model may be able to more closely resemble the decay rates that are seen in the actual PRS of Fig. 3. Though our four-state model does exhibit

behavior helps explain how the extended tails come about, there still are adjustments required in order to quantitatively replicate the map-based PRS. For example, a model with a larger set of states that mimic the actual phase space should give a more quantitative agreement: this is the idea behind the Ulam method,[41] which approximates the Perron-Frobenius operator by discretizing the phase space. However, any such a finite discretization could not fully respect the fractal nature of the invariant subsets of the true dynamics, nor will it be able to exhibit the power-law decay expected for the deterministic case.

While the noise-enhanced stickiness we have observed here should be a generic phenomenon in area-preserving maps, it would interesting to study the effect of noise on higher-dimensional volume-preserving dynamics, such as the ABC map. Such systems can model mixing of passive scalars in an incompressible flow.

Appendices

Appendix A: Varying the Noise Distribution

The computations in §III and §IV used Gaussian noise, (5) applied independently to each component of the map (3). To check how the results depend upon the noise distribution, we consider two additional cases in this appendix:

- Uniform noise on a box with sides $[-R, R]$, i.e., choose independent

$$\delta x, \delta y \sim \mathcal{U}([-R, R]), \tag{A1}$$

  with variances $\sigma^2 = R/\sqrt{3}$. This was also used by da Silva, Manchein, and Beims[15].

- Post hoc noise, i.e., added after the deterministic iteration of (2),

$$f_{PH}(x, y) = H(x, y) + (\delta x, \delta y). \tag{A2}$$

  In this case we choose $\delta x, \delta y \sim \mathcal{N}(0, \sigma^2)$, the Gaussian distribution, recall (5).

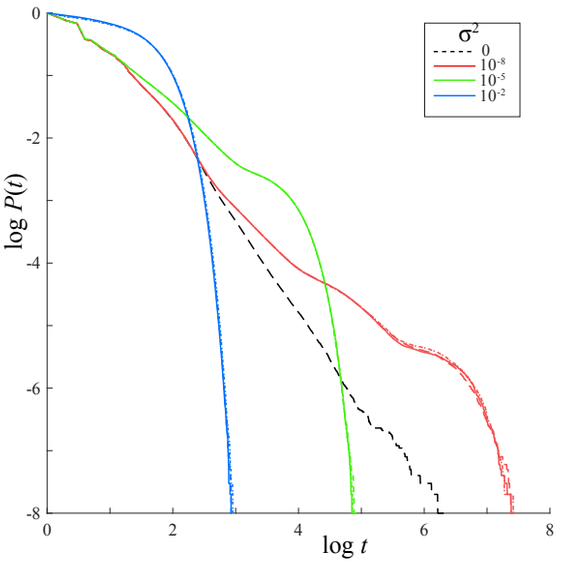

FIG. 11: Comparison of the PRS for (2) with $(K, L) = (0.6, 4.0)$ and three types of noise: Gaussian (5) (short dashes), uniform (A1) (long dashes) and post hoc (A2) (solid) for three values of the variance.

Of course other distributions are possible for additive noise, and it is also possible to have noise that varies the parameters[42,43] or even the structure of the map; however, we did not consider these additional cases.

The effect on $P(t)$ of changing the noise distribution to uniform noise (A1) was shown in Fig. 2(b) for $(K, L) = (0.6, 4)$ and for the same values of the variance that we used for the normally distributed noise in Fig. 2(a). The two sets of curves for panels (a) and (b) are very close; the differences that do appear are most prominent when $P(t) \lesssim 10^{-6}$, but these statistical errors can be expected since there are few surviving trajectories for these large times.

The three noise varieties are compared for $(K, L) = (0.6, 4)$ in Fig. 11. Here, the solid curves represent post hoc noise (A2), and the dashed curves are the Gaussian and uniform cases from Fig. 2. The biggest differences occur for the smallest variance, $\sigma^2 = 10^{-8}$ and these are only visible in the figure for $P(t) \lesssim 10^{-5}$ where sampling errors can be expected.

Similar results were also obtained for $(K, L) = (1, 5)$ (not shown).

We can conclude that the three noise methods are equivalent, at least for the PRS and

the timescales of our computations.

Appendix B: PRS Decay Rates

In Table I we report fits to a power law (14), or to an exponential decay (15) for the PRS shown in Fig. 2(a). The power law applies for short times and this is replace by an exponential decay for longer times when there is noise. The power law exponent γ and the exponential rate α were obtained using least squares fits to the log-log or log-linear $P(t)$ data, respectively, over the time intervals indicated in columns two and four. The error bounds, shown in parentheses for the last digit, represent the least squares errors in the slopes. The deterministic case has no exponential interval, and the fitted power law is close to the value, $\gamma \simeq 1.56$, expected to be universal for area-preserving maps.[8,35,37] The the two largest noise levels, $\sigma^2 = 10^{-2}$ and 10^{-1}, have no power-law interval.

σ^2	$\log t$ range	γ	$\log t$ range	α
0	$[1.00, 5.00]$	1.5587(3)	–	–
10^{-8}	$[2.85, 5.55]$	0.7593(1)	$[6.10, 6.79]$	$2.59374(3) \times 10^{-7}$
10^{-7}	$[2.61, 4.68]$	0.7767(2)	$[5.09, 6.28]$	$2.32201(7) \times 10^{-6}$
10^{-6}	$[1.66, 3.65]$	0.879(1)	$[4.33, 5.56]$	$2.0110(1) \times 10^{-5}$
10^{-5}	$[0.95, 2.85]$	0.942(2)	$[3.52, 4.75]$	$1.6765(1) \times 10^{-4}$
10^{-4}	$[0.85, 2.38]$	0.803(5)	$[2.82, 3.91]$	$1.21597(6) \times 10^{-3}$
10^{-3}	$[0.85, 1.74]$	0.580(7)	$[2.12, 3.26]$	$6.986(1) \times 10^{-3}$
10^{-2}	–	–	$[1.42, 2.82]$	$2.0054(4) \times 10^{-2}$
10^{-1}	–	–	$[1.42, 2.71]$	$2.5599(7) \times 10^{-2}$

TABLE I: Power-law (14) and exponential (15) fits to the PRS from Fig. 2(a) for the Harper map with $(K, L) = (0.6, 4.0)$ and Gaussian noise (5) with variance σ^2.

For the case $(K, L) = (1, 5)$ shown in Fig. 3(a), $P(t)$ appears to decay as a sum of exponentials, and fits to the two exponential rates, α_1 and α_2, and the time intervals over

which they apply are given in Table II. Note that these exponential fits apply even to the deterministic case: since the elliptic islands in the phase space—recall Fig. 1(a)—are small, the expected, asymptotic power law apparently occurs only on longer time scales than our simulations. Similar hyper-exponential distributions have been reported for other maps.[38]

σ^2	$\log t$ range	α_1	$\log t$ range	α_2
0	$[0.00, 1.98]$	$4.67(4) \times 10^{-2}$	$[2.60, 4.08]$	$8.5242(6) \times 10^{-4}$
10^{-8}	$[0.70, 1.79]$	$4.46(5) \times 10^{-2}$	$[2.47, 3.95]$	$7.885(5) \times 10^{-4}$
10^{-7}	$[0.30, 1.83]$	$4.33(5) \times 10^{-2}$	$[2.77, 4.06]$	$8.965(1) \times 10^{-4}$
10^{-6}	$[0.30, 1.86]$	$4.18(5) \times 10^{-2}$	$[2.62, 4.04]$	$9.9472(6) \times 10^{-4}$
10^{-5}	$[0.30, 1.75]$	$4.31(5) \times 10^{-2}$	$[2.63, 3.79]$	$1.6872(1) \times 10^{-3}$
10^{-4}	$[0.30, 1.60]$	$3.93(7) \times 10^{-2}$	$[2.27, 3.29]$	$5.4444(7) \times 10^{-3}$
10^{-3}	$[1.78, 2.92]$	$1.4081(1) \times 10^{-2}$	–	–
10^{-2}	$[1.42, 2.79]$	$2.1664(3) \times 10^{-2}$	–	–
10^{-1}	$[0.00, 2.72]$	$2.5584(6) \times 10^{-2}$	–	–

TABLE II: Exponential fits to the PRS from Fig. 3(a) for the Harper map with $(K, L) = (1, 5)$ and Gaussian noise (5) with variance σ^2. The two rates, α_1 and α_2, apply for the $\log t$ intervals shown. For $\sigma^2 = 10^{-8}$ there is a third rate, (B1), on the longest time scale.

Note that when $\sigma^2 < 10^{-6}$ in Table II, the rates α_1 and α_2 are close to the deterministic case. Though this is still true when $\sigma^2 = 10^{-8}$, in this case $P(t)$ has a third exponential rate (not shown in Table II) with

$$\alpha_3 = 1.1838(3) \times 10^{-4}, \quad \sigma^2 = 10^{-8}\,, \tag{B1}$$

for $4.12 < \log t < 4.56$. This corresponds to the extended tail visible in Fig. 3(a) when compared to the deterministic case. By contrast, for the largest variances, $\sigma^2 \geq 10^{-3}$, we observe only a single exponential rate, and thus the column for α_2 in the table is empty.

ACKNOWLEDGMENTS

Support from a gift from the Northrop-Grumman University Research fund is gratefully acknowledged. The authors would like to thank the referees for their helpful comments.

REFERENCES

[1]V. Arnold, "Instability of dynamical systems with several degrees of freedom," Sov. Math. Dokl. **5**, 581–585 (1964).

[2]P. Lochak, "Canonical perturbation theory via simultaneous approximation," Russ. Math. Surv. **47**, 59–140 (1992).

[3]R. MacKay, J. Meiss, and I. Percival, "Transport in Hamiltonian systems," Physica D **13**, 55–81 (1984).

[4]J. Meiss, "Symplectic maps, variational principles, and transport," Rev. Mod. Phys. **64**, 795–848 (1992).

[5]J. Meiss, "Thirty years of turnstiles and transport," Chaos **25**, 097602 (2015).

[6]C. Karney, "Long time correlations in the stochastic regime," Physica D **8**, 360–380 (1983).

[7]B. Chirikov and D. Shepelyansky, "Correlation properties of dynamical chaos in Hamiltonian systems," Physica D **13**, 395–400 (1984).

[8]J. Meiss and E. Ott, "Markov tree model of intrinsic transport in Hamiltonian systems," Phys. Rev. Lett. **55**, 2741–2744 (1985).

[9]S. Lange, A. Bäcker, and R. Ketzmerick, "What is the mechanism of power-law distributed Poincaré recurrences in higher-dimensional systems?" Europhys. Lett. **116**, 30002 (2016).

[10]M. Sales, M. Mugnaine, J. Szezech, J.D., R. Viana, I. Caldas, N. Marwan, and J. Kurths, "Stickiness and recurrence plots: An entropy-based approach," Chaos **33**, 033140 (2023).

[11]B. Chirikov, "Homogeneous model for resonant particle diffusion in an open magnetic confinement system," Sov. J. Plas. Phys. **5**, 492–497 (1979).

[12]A. Rechester and R. White, "Calculation of turbulent diffusion for the Chirikov-Taylor model," Phys. Rev. Lett. **44**, 1586–1589 (1980).

[13]C. Karney, A. Rechester, and R. White, "Effect of noise on the standard mapping," Physica D **4**, 425–438 (1982).

[14]I. Mezíc and S. Wiggins, "Nonergodicity, accelerator modes, and asymptotic quadratic-in-time diffusion in a class of volume-preserving maps," Phys. Rev. E **52**, 3215–3217 (1995).

[15]R. da Silva, C. Manchein, and M. Beims, "Exploring conservative islands using correlated and uncorrelated noise," Phys. Rev. E **97**, 022219 (2018).

[16]M. Demers, P. Wright, and L.-S. Young, "Escape rates and physically relevant measures for billiards with small holes," Comm. Math. Phys. **294**, 353–388 (2010).

[17]J. Bernal, J. Seoane, and M. F. Sanjuán, "Weakly noisy chaotic scattering," Phys. Rev. E **88**, 032914 (2013).

[18]A. Nieto, J. Seoane, and M. Sanjuán, "Noise activates escapes in closed Hamiltonian systems," Comm. Nonlin. Sci. Num. Sim. **105**, 106074 (2022).

[19]E. Altmann and T. Tél, "Poincaré recurrences and transient chaos in systems with leaks," Phys. Rev. E **79**, 016204 (2009).

[20]A. Bazzani, S. Siboni, and G. Turchetti, "Action diffusion for symplectic maps with a noisy linear frequency," J. Phys. A **30**, 27 (1997).

[21]E. Ott, E. Yorke, and J. Yorke, "A scaling law: How an attractor's volume depends on noise level," Physica D **16**, 62–78 (1985).

[22]E. Altmann and A. Endler, "Noise-enhanced trapping in chaotic scattering," Phys. Rev. Lett. **105**, 244102 (2010).

[23]J. Seoane, L. Huang, M. Sanjuán, and Y.-C. Lai, "Effect of noise on chaotic scattering," Phys. Rev. E **79**, 047202 (2009).

[24]M. Ohshika, D. Lippolis, and A. Shudo, "Escape-rate response to noise of all amplitudes in leaky chaos," Physica D **458**, 134016 (2024), https://doi.org/10.1016/j.physd.2023.134016.

[25]P. Lebœuf, "Normal and anomalous diffusion in a deterministic area-preserving map," Physica D **116**, 8–20 (1998).

[26]S. Shinohara, "The threshold for global diffusion in the kicked Harper map," Phys. Lett. A **298**, 330–334 (2002).

[27]R. Mitchell and J. Meiss, "Designing a finite-time mixer: Optimizing stirring for two-dimensional maps," SIAM J. Dyn. Syst. **16**, 1514–1542 (2017).

[28]C. Karney, "Stochastic heating by a lower hybrid wave II," Phys. Fluids **22**, 2186–2209 (1979).

[29]R. Artuso, G. Casati, F. Borgonovi, L. Rebuzzini, and I. Guarneri, "Fractal and dynamical properties of the kicked Harper model," Int. J. Mod. Phys. B **08**, 207–235 (1994).

[30]M. Liu, F. Muzzio, and R. Peskin, "Quantification of mixing in aperiodic chaotic flows," Chaos, Solitons and Fractals **4**, 869–893 (1994).

[31]A. Saito, Y. Nomura, K. Hirose, and Y. Ichikawa, "Separatrix reconnection and periodic orbit annihilation in the Harper map," Chaos **7**, 245–253 (1997).

[32]R. Artuso, "Correlation decay and return time statistics," Physica D **131**, 68–77 (1999).

[33]B. Chirikov and D. Shepelyansky, "Asymptotic statistics of Poincaré resurrences in Hamiltonian systems with divided phase space," Phys. Rev. Lett. **82**, 528–531 (1999).

[34]E. Altmann, A. Motter, and H. Kantz, "Stickiness in Hamiltonian systems: From sharply divided to hierarchical phase space," Phys. Rev. E **73**, 026207 (2006).

[35]G. Cristadoro and R. Ketzmerick, "Universality of algebraic decays in Hamiltonian systems," Phys. Rev. Lett. **100**, 184101 (2008).

[36]J. Meiss, "Average exit time for volume-preserving maps," Chaos **7**, 139–147 (1997), https://doi.org/10.1063/1.166245.

[37]O. Alus, S. Fishman, and J. Meiss, "Universal exponent for transport in mixed Hamiltonian dynamics," Phys. Rev. E **96**, 032204 (2017).

[38]C. Lozej, "Stickiness in generic low-dimensional Hamiltonian systems: A recurrence-time statistics approach," Phys. Rev. E **101**, 052204 (2020).

[39]E. Floriani, R. Mannella, and P. Grigolini, "Noise-induced transition from anomalous to ordinary diffusion: The crossover time as a function of noise intensity," Phys. Rev. E **52**, 5910–5917 (1995).

[40]R. Ishizaki, H. Shibata, and H. Mori, "Effects of external noise on anomalous diffusion in Hamiltonian dynamical systems," Prog. Theor. Phys. **103**, 245–259 (2000).

[41]G. Froyland, "Using Ulam's method to calculate entropy and other dynamical invariants,"

Nonlinearity **12**, 79–101 (1999).

[42]C. Rodrigues, A. de Moura, and C. Grebogi, "Random fluctuation leads to forbidden escape of particles," Phys. Rev. E **82**, 027211 (2010).

[43]F. Bouchet and E. Woillez, "Transport in Hamiltonian systems with slowly changing phase space structure," Comm. Nonlin. Sci. Num. Sim. **80**, 104935 (2020).